




# Evaluating semi-analytical algorithms for estimating inherent optical properties in the South China Sea

LIN DENG,<sup>1,2</sup>  WEN ZHOU,<sup>1,3,4,\*</sup> WENXI CAO,<sup>1,3,4</sup> GUIFEN WANG,<sup>5</sup> WENDI ZHENG,<sup>1,2</sup> ZHANTANG XU,<sup>1,3</sup> CAI LI,<sup>1,3</sup> YUEZHONG YANG,<sup>1,3</sup> WENLONG XU,<sup>5</sup> KAI ZENG,<sup>1,2</sup> AND SHUIBO HU<sup>6</sup>

<sup>1</sup>State Key Laboratory of Tropical Oceanography, South China Sea Institute of Oceanology, Chinese Academy of Sciences, Guangzhou 510301, China

<sup>2</sup>University of Chinese Academy of Sciences, Beijing 100049, China

<sup>3</sup>Southern Marine Science and Engineering Guangdong Laboratory, Guangzhou 510301, China

<sup>4</sup>Guangdong Key Lab of Ocean Remote Sensing, Guangzhou 510301, China

<sup>5</sup>College of Oceanography, Hohai University, Nanjing 210098, China

<sup>6</sup>College of Life Sciences and Oceanography, Shenzhen University, Shenzhen 518060, China

\*wenzhou@scsio.ac.cn

**Abstract:** Using large amounts of bio-optical data collected in the South China Sea (SCS) from 2003 to 2016, this study checks the consistency between well-known semi-analytical algorithms (SAAs)—the quasi-analytical algorithm (QAA) and the default generalized inherent optical property (GIOP-DC)—in retrieving the non-water absorption coefficient ( $a_{nw}(\lambda)$ ), phytoplankton absorption coefficient ( $a_{ph}(\lambda)$ ) and particulate backscattering coefficient ( $b_{bp}(\lambda)$ ) from remote-sensing reflectance ( $R_{rs}(\lambda)$ ) data at 412, 443, 490, 531, and 555 nm. The samples from the SCS are further separated into oligotrophic and mesotrophic water types for the comparison of the SAAs. Several findings are made: First, the values of  $a_{nw}(\lambda)$  derived from the two SAAs deliver similar performance, with  $R^2$  values ranging from 0.74 to 0.85 and 0.74 to 0.87, implying absolute percent error differences (APDs) from 37.93% to 74.88% and from 32.32% to 71.75% for the QAA and GIOP-DC, respectively. The QAA shows a value of  $R^2$  between 0.64 and 0.91 and APDs between 43.57% to 83.53%, while the GIOP-DC yields  $R^2$  between 0.76 to 0.89 and APDs between 44.65% to 79.46% when estimating  $a_{ph}(\lambda)$ . The values of  $b_{bp}(\lambda)$  derived from the QAA are closer to the in-situ  $b_{bp}(\lambda)$  values, as indicated by the low values of the normalized centered root-mean-square deviation and normalized standard deviation, which are close to one. Second, a regionally tuned estimation of  $a_{ph}(\lambda)$  is proposed and recommended for the SCS. This consistency check of inherent optical properties products from SAAs can serve as reference for algorithm selection for further applications, including primary production, carbon, and biogeochemical models of the SCS, and can provide guidance for improving  $a_{ph}(\lambda)$  estimation.

© 2020 Optical Society of America under the terms of the [OSA Open Access Publishing Agreement](#)

## 1. Introduction

Inherent optical properties (IOPs) encompass the absorption and scattering properties of seawater as well as its particulate and dissolved constituents. Understanding oceanic responses to the varying and changing climate is critical to maintaining the Earth as a habitable planet, and requires substantial volumes of information from marine-biological and biogeochemical processes [1]. In practice, the components of IOPs, associated with different constituents of seawater—phytoplankton, non-algal particles, and colored dissolved organic matter—can provide critical information about properties of the ocean and its biogeochemical processes [2]. Thus, the description and prediction of changes in marine IOPs are critical goals for many fields in oceanography.

Satellite remote sensing is a powerful and the only tool available to estimate IOPs with high spatial coverage and temporal resolution. To make use of this capability, robust inverse algorithms need to be established. In the past two decades, several semi-analytical algorithms (SAAs) have been developed and used to estimate IOPs from remote sensing reflectance ( $R_{rs}(\lambda)$ ) [2–9]. There are three widely used SAAs: the quasi-analytical algorithm (QAA), Garver–Siegel–Maritorena (GSM) method, and generalized IOP algorithm (GIOP), initially proposed by Lee et al. [8], Garver and Siegel et al. [5], and Werdell et al. [2], respectively.

Efforts are ongoing to compare SAA-derived IOPs to in-situ IOPs in different regions of the sea. For examples, Chen et al. [10] showed that the mean absolute percent error differences (APDs) between the total absorption coefficient ( $a(443)$ ) and backscattering coefficient at 443 nm ( $b_b(443)$ ) derived from QAA and in-situ measurements in the Eastern China Sea including Bohai Sea, Yellow Sea, and East China Sea, were 15.8% and 17.8%, respectively. Zheng et al. [11] used concurrent measurements of IOPs and apparent optical properties (AOPs) in Arctic waters to evaluate the total absorption and backscattering as well as their components using the QAA. They reported that the mean relative percent differences between  $a(443)$  and  $b_b(443)$  derived from the QAA and in-situ measurements were 10.44% and 8.25%, respectively. Moreover, consistency checks of SAAs have been conducted in the coastal waters of Korea, coastal Yellow Sea, and East China Sea [12,13]. Shanmugam et al. [13] examined the overall performance of the SAAs around coastal Korean waters, and showed that the over-constrained linear matrix inversions (LM) > GSM > QAA for retrieving  $a_{ph}(\lambda)$ , LM > GSM > QAA for retrieving  $a_{dg}(\lambda)$ , and QAA > GSM > LM for retrieving  $b_{bp}(\lambda)$ . Likewise, Huang et al. [12] reported that the QAA delivered the best performance in the retrieval of all coefficients, and the GSM yielded the largest fluctuations for absorption coefficient retrievals in the coastal Yellow Sea and East China Sea.

As the performances of SAAs vary considerably across oceans, consistency of SAAs must be checked in specific areas to ensure algorithm robustness when retrieving the desired products so that certain derivations of the SAAs can be accurately used for further study. If data from shallower oceans are used, the differences between the estimated IOPs and in-situ measurements are generally higher. Regardless of the amount of effort, in-situ measurements are always hampered by coverage, both in time and space, which may lead to unreliable assessments. Comparisons of SAA-derived IOP products based on these limited datasets provide little information about the applicability of SAAs to the South China Sea (SCS) and about the biogeochemical model. The number of in-situ measurements used in these studies are small and beyond the SCS.

The SCS is the largest marginal sea of the western Pacific Ocean, covering about 3.5 million square kilometers and containing many complex dynamic processes, including monsoons, its circulation, mesoscale eddies, and upwelling [14,15]. These dynamic processes cause complex bio-optics in the SCS that hamper the application of retrieval algorithms. Bio-optical properties, especially phytoplankton communities in the SCS, have been investigated using long-term datasets [16–18]. In general, the SCS shows oligotrophic characteristics as it is abundant in pico-phytoplankton (60% to 95%), whereas the Pearl River plume and waters near the shore are eutrophic, dominated by micro-phytoplankton (> 80%) [16]. To the best of our knowledge, the IOP products of SAAs have not been adequately compared in the SCS, and this has far-reaching implication for primary production and the carbon model. Thus, it is important to check the consistency of SAAs in the SCS. To address this, we collected a bio-optical dataset from 13 cruises between 2003 and 2016 in the SCS. The dataset contained concurrent field-measured AOPs and IOPs, such as match-ups of  $R_{rs}(\lambda)$  and the phytoplankton absorption coefficient ( $a_{ph}(\lambda)$ ), match-ups of  $R_{rs}(\lambda)$  and the non-water absorption coefficient ( $a_{nw}(\lambda)$ ), and those of  $R_{rs}(\lambda)$  and the particulate backscattering coefficient ( $b_{bp}(\lambda)$ ). Note that the GSM is a special type of GIOP if the selection of parameters of the GIOP is in keeping with those of the GSM. Thus, for simplicity, only QAA and GIOP have been selected for comparison. The objectives of this study are to: (1) check the consistency of the SAAs over the SCS, and provide relatively

accurate statistical differences for the retrieval of  $a_{ph}(\lambda)$ ,  $a_{nw}(\lambda)$ , and  $b_{bp}(\lambda)$  relative to in-situ measurements; (2) classify water types based on the field  $R_{rs}(\lambda)$  spectrum and compare retrievals of the SAAs to in-situ measurements in oligotrophic and mesotrophic waters; and (3) provide discussions on how to improve estimate of  $a_{ph}(\lambda)$  in the SCS.

## 2. Materials and methods

Using data obtained from 13 cruises, concurrent bio-optical field data of IOPs and AOPs were collected from the SCS from 2003 to 2016 to check the consistency of SAAs (Fig. 1 and Table 1). The field data of the SCS were collected mostly in open ocean waters of the SCS, with a smaller number of in-situ measurements collected in the shelf region. Moreover, most field data were collected from August to October, and data from only one cruise in the central SCS were collected in April, 2010. After careful examination of these data, 194 samples of  $a_{ph}(\lambda)$ , 56 samples of  $a_{nw}(\lambda)$ , and 21 samples of  $b_{bp}(\lambda)$  and their corresponding  $R_{rs}(\lambda)$  from surface water were selected.

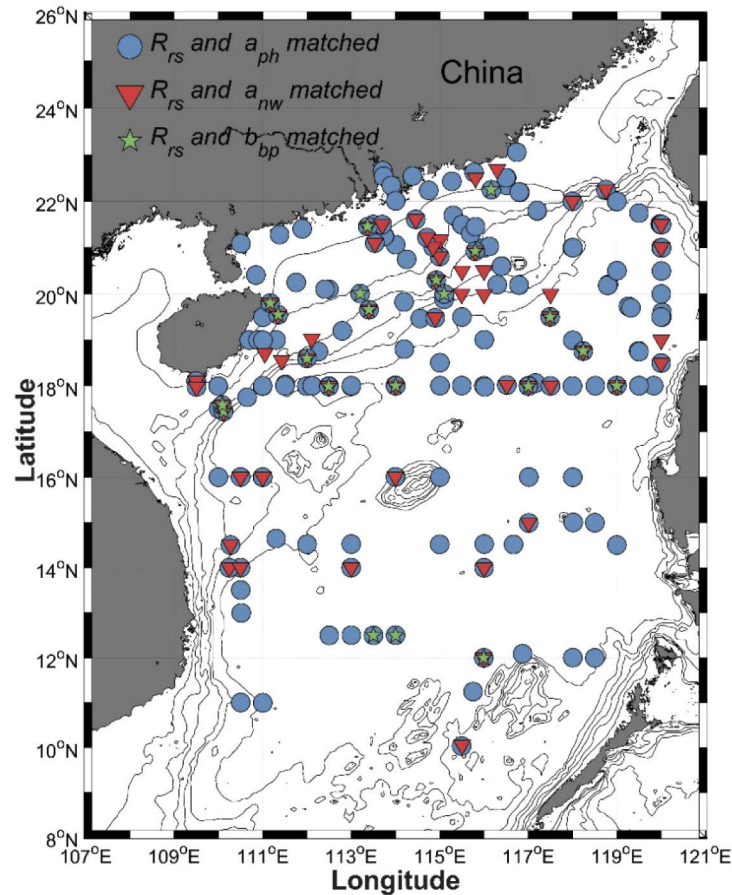


**Fig. 1.** Locations of match-ups of  $R_{rs}(\lambda)$  and  $a_{ph}(\lambda)$  (blue squares),  $R_{rs}(\lambda)$  and  $a_{nw}(\lambda)$  (red triangles), and match-ups of  $R_{rs}(\lambda)$  and  $b_{bp}(\lambda)$  (green pentagrams). The upward direction is due north.

Table 1. Summary of datasets used in this study.

Expedition	Date	Location	$R_{rs}$	$a_{nw}$	$a_{ph}$	$b_{bp}$	N (Meso)	N (Match)
CWGD_2003	October 2003	Costal water of Guangdong	✓		✓		4	12
NSCS_2004	September 2004	Northern South China Sea	✓		✓		1	13
NSCS_2005	September 2005	Northern South China Sea	✓		✓		2	16
NSCS_2006	September 2006	Northern South China Sea	✓		✓		3	19
NSCS_2007	August 2007	Northern South China Sea	✓		✓		1	12
NSCS_2008	August 2008	Northern South China Sea	✓	✓	✓		0	14
NSCS_2009	September 2009	Northern South China Sea	✓		✓		0	9
CSCS_2010	April 2010	Central South China Sea	✓		✓		0	32
NSCS_2011	September 2011	Northern South China Sea	✓		✓		1	16
SCS_2012	December 2012	Central South China Sea	✓	✓	✓		0	18
NESCS_2013	October 2013	Northeastern South China Sea	✓		✓	✓	3	7
NESCS_2015	June 2015	Northeastern South China Sea	✓	✓	✓	✓	5	16
CSCS_2016	September 2016	Central South China Sea	✓	✓	✓	✓	0	8

### 2.1. Measurement of $R_{rs}$

During the 2003–2012 cruises, the Satlantic Profiling Multichannel Radiometer (Satlantic Inc., Halifax, Canada) was deployed to measure vertical profiles of downwelling irradiance ( $E_d(\lambda, z)$ ) and upwelling radiance ( $L_u(\lambda, z)$ ) at seven bands (412, 443, 490, 520, 555, 620 and 683 nm) simultaneously. In the 2013, 2015 and 2016 cruises,  $L_u(\lambda, z)$  and  $E_d(\lambda, z)$  were measured using a free-fall hyperspectral profiling radiometer (HyperPro, Satlantic Inc.), which covers a spectral range from 350–800 nm at intervals of 3.3 nm.  $R_{rs}(\lambda)$  was calculated from  $L_u(\lambda, z)$  and  $E_d(\lambda, z)$  by software provided by the instrument manufacturers (ProSoft 7.7.16). Errors in  $R_{rs}(\lambda)$  from field measurements were related to instrument platforms, strategies of deployment, data processing, and the ambient environments [19–21]. Thus, the radiometer measurements and data processing followed the NASA ocean optics protocols [19].

### 2.2. Measurement of inherent optical properties

In our study, the values of  $a_w(\lambda)$  were obtained from [22], while  $a_{ph}(\lambda)$  was calculated by subtracting  $a_d(\lambda)$  from  $a_p(\lambda)$ . The particulate backscattering coefficients ( $b_{bp}(\lambda)$ ) were obtained by subtracting the backscattering coefficients by seawater ( $b_{bsw}(\lambda)$ ) [23] from the total backscattering coefficients ( $b_b(\lambda)$ ).

At all cruises from 2003 to 2016,  $a_{ph}(\lambda)$  was measured using the quantitative filter-pad technique (QFT) [24,25]. Water samples were collected using Niskin bottles in discrete layers within the photic zone. A suitable volume of water (0.5–4 L), depending on the quantity of the particles, was filtered onto a 25-mm, 0.7- $\mu$ m Whatman GF/F glass fiber filter at low vacuum to record  $a_p(\lambda)$ . The filters were kept into a dark liquid nitrogen container for a maximum of two months until laboratory analysis. In the laboratory,  $a_p(\lambda)$  was measured using a dual-beam UV–visible spectrophotometer (UV-2550, Shimadzu Corp., Japan) between 350 nm and 750 nm at a resolution of 1 nm. Then, to eliminate the phytoplankton pigment, the filters were extracted with methanol for 90–180 min [7]. The filters were rescanned using a spectrophotometer to obtain  $a_d(\lambda)$  using the same method. To correct the scattering signal, all spectra were shifted by subtracting the absorption at 750 nm [26,27]. The path-length amplification effect was corrected corresponding to the method proposed by Stramski et al. [28]. Finally,  $a_{ph}(\lambda)$  was determined by the difference between  $a_p(\lambda)$  and  $a_d(\lambda)$  [29,30].

$a_{nw}(\lambda)$  was measured by commercial hydrologic optical instruments (e.g., ACS and AC9, the nine-wavelength and hyperspectral versions, respectively (WET Labs Inc.)) during four cruises from 2008 to 2016. On cruises to the Northern South China Sea (NSCS) (October 2008 and 2012), the absorption and attenuation coefficients were measured by the AC9 meter at nine wavelengths (412, 449, 488, 510, 532, 555, 630, 676, and 715 nm). On the NSCS cruise and the northeastern South China Sea (NESCS) cruise (August–October 2015 and 2016, respectively), the ACS was used to measure  $a_{nw}(\lambda)$  over 82 wavelengths between 401.6 and 744.1 nm with a path length of 25 cm. Calibrations with pure water were conducted to correct the drift of the instrument and eliminate the absorption of pure water from the measured records. The values of pure water were within  $0.005 \text{ m}^{-1}$  absorption and within  $0.01 \text{ m}^{-1}$  attenuation of the calibration values, consistent with factory designation instrumental noise [31]. The effects of temperature and salinity on absorption and attenuation were corrected using measurement by conductivity temperature depth (CTD) [32]. To correct for the incomplete recovery of scattered light, three methods are commonly used, as described in the AC-9 and AC-S manuals: for example, subtracting the absorption measured at a reference wavelength, where the absorption is assumed to be zero, or by removing a fixed proportion of the scattering coefficient. Additionally, some scattering-correction methods have been developed based on 3D Monte Carlo simulations [33,34]. In our study, the absorption measurements at 715 nm were subtracted over each measured visible spectrum for AC-9. For the sake of consistency, the average absorption value at the same wavelength (715 nm) was also subtracted over the measured spectra for AC-S [35].

During the NSCS and NESCS cruises (August–October 2013, 2015, and 2016),  $b_{bp}(\lambda)$  was measured with HS6 (HydroScat-6, HOBI Labs, Inc.). It measured the volume of the scattering function at a scattering angle centered at  $140^\circ$  ( $\beta(140^\circ, \lambda)$ ) at six wavelengths (420, 442, 488, 532, 590 and 676 nm), which was transformed into  $b_{bp}(\lambda)$  through a coefficient of 1.1 [36]. The pure seawater backscattering coefficient ( $b_{bsw}(\lambda)$ ) was obtained from Zhang et al. [23]. A sigma correction was performed to correct the path length attenuation effects (HOBI Laboratories, Incorporated, 2012). After the correction of the raw data, the profile data of  $a_{nw}(\lambda)$  and  $b_{bp}(\lambda)$  were split into down-cast and up-cast. To obtain in-situ measurements of the spectral slopes of  $b_{bp}(\lambda)$  and  $b_{bp}(\lambda)$  in an arbitrary spectrum, a power function, using the relation  $b_{bp}(\lambda) = b_{bp}(\lambda_0) \times (\lambda_0/\lambda)^\eta$ , was fitted to the spectral data of  $b_{bp}(\lambda)$  measured at discrete wavelengths with a reference wavelength of 532 nm.

### 2.3. Semi-analytical algorithms

Several SAAs have been proposed to derive IOPs from sensor-observed  $R_{rs}(\lambda)$  using a combination of empiricism and radiative transfer theory [37]. Gordon et al. [38] established the relation between IOPs and AOPs through the analysis of radiance transfer theory and simulations:

$$r_{rs}(\lambda) = g_1 u(\lambda) + g_2 [u(\lambda)]^2, \quad (1)$$

$$u(\lambda) = \frac{b_b(\lambda)}{a(\lambda) + b_b(\lambda)}, \quad (2)$$

$$r_{rs}(\lambda) = \frac{R_{rs}(\lambda)}{0.52 + 1.7R_{rs}(\lambda)}, \quad (3)$$

where  $r_{rs}(\lambda)$  is used regularly to represent remote-sensing reflectance below the sea surface as calculated by Eq. (3).  $U(\lambda)$  represents the function of IOPs, where  $g_1 = 0.0949 \text{ (sr}^{-1}\text{)}$ , and  $g_2 = 0.0794 \text{ (sr}^{-1}\text{)}$ . Two strategies, a bottom-up and a top-down strategy, were applied to derive the IOPs by using the SAAs. The QAA applied top-down strategies to derive  $a(\lambda)$  and  $b_b(\lambda)$  first from the input of  $R_{rs}(\lambda)$  using a reference wavelength at 555 nm or 670 nm. Then, the QAA separated  $a_{ph}(\lambda)$  and non-phytoplankton materials ( $a_{dg}(\lambda)$ ) using the empirically assumed spectral slope of  $a_{dg}(\lambda)$  ( $S_{dg}$ ). Note that the GIOP and GSM, however, applied bottom-up strategies on



in-situ  $R_{rs}(\lambda)$  to retrieve the IOPs by assuming the normalized spectral absorption coefficients (shape;  $a^*$ ) of  $a_{dg}(\lambda)$ ,  $b_{bp}(\lambda)$ , and  $a_{ph}(\lambda)$ . The magnitudes of each component were optimized using nonlinear least-squares Levenberg–Marquardt optimization by using assumed starting point and up–low bounds on the variable. A simplified flowchart of the three SAAs is shown in Fig. 2.

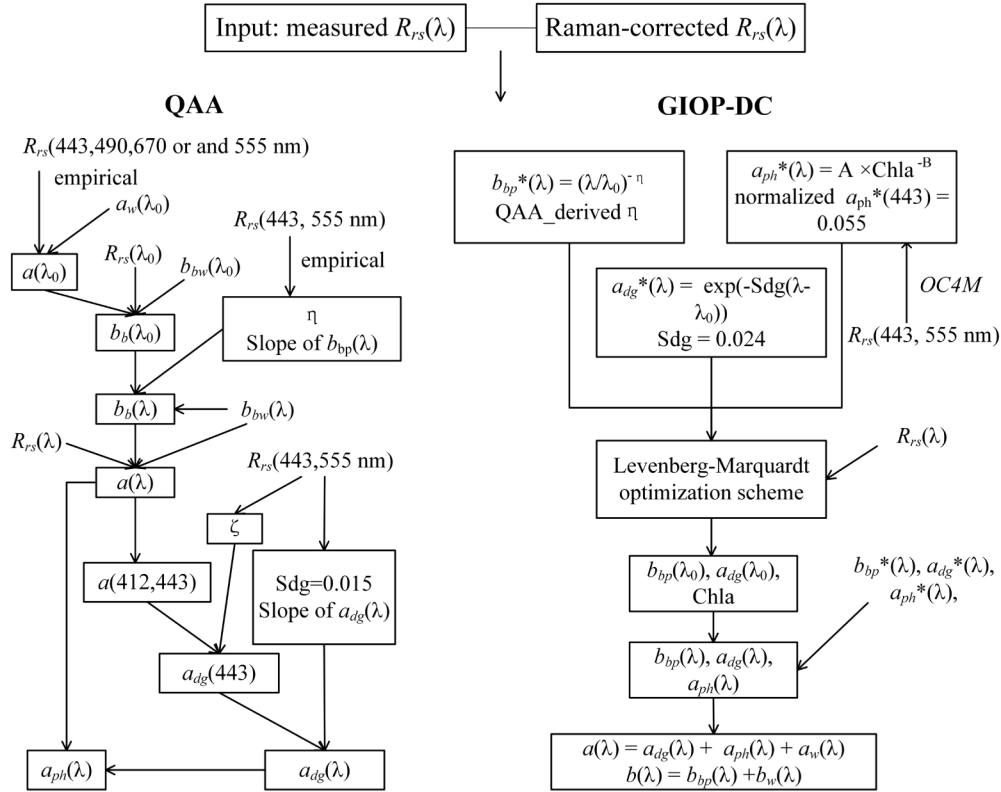


**Fig. 2.** Schematic flows of QAA and GIOP-DC.

The QAA was developed by Lee et al. [8] and has been modified several times since [39–42]. In our study, the current version 6 of the QAA (QAA\_v6) was used (codes created by Jianwei Wei, UMass Boston). The important modification to the QAA\_v6 makes use of the optional reference waveband according to the values of  $R_{rs}$  (670) ( $< 0.0015 \text{ sr}^{-1}$ , select 550 nm and  $> 0.0015 \text{ sr}^{-1}$ , select 670 nm as reference). For  $R_{rs}$  (670) larger than 0.0015, the quality of  $R_{rs}$  (670) is acceptable, which makes it possible to set it as reference waveband in the QAA. However, note that almost all values of our  $R_{rs}$  (670) were smaller than  $0.0015 \text{ sr}^{-1}$ .

The GSM was proposed by Garver and Siegel [5] and modified by Maritorena et al. [9]. The GIOP was proposed by Werdell et al. [2], and provides a framework of IOP algorithms that incorporate several selections from an assortment of published bio-optical models and model parameterizations, allowing users to select and evaluate the model for their particular environments. That is to say, the GSM is a special type of GIOP if the selections of parameters of the GIOP are keeping with those of the GSM. For comparison, the default configuration of the GIOP proposed by the NASA GIOP workshops were utilized as a general type of GIOP in this study—hereinafter denoted by GIOP default configuration (GIOP-DC).

Both the GSM and the GIOP-DC use  $R_{rs}(\lambda)$  as input, assign constant values to  $a_w(\lambda)$  and  $b_{bsw}(\lambda)$  [43], assume spectral shapes for non-water constituents, and derive the magnitudes of absorption and backscattering constituents via the nonlinear least-squares Levenberg–Marquardt

optimization scheme. The core solution methods of GSM and GIOP-DC are identical with two primary differences in the assumptions to determine the spectral shapes of  $a_{ph}(\lambda)$  and  $a_{dg}(\lambda)$  ( $a_{ph}^*(\lambda)$  and  $a_{dg}^*(\lambda)$ ). In the GSM,  $a_{ph}^*(\lambda)$  is set to constant values [0.00665, 0.05582, 0.02055, 0.01910, 0.01015, 0.01424] at the six wavelengths, respectively and  $a_{ph}^*(443)$  is specified as  $0.055 \text{ m}^2 \text{ mg Chla}^{-1}$ ; the spectral slope of  $a_{dg}(\lambda)$  ( $S_{dg}$ ) is parameterized as  $0.02061 \text{ nm}^{-1}$ . In the GIOP-DC,  $a_{ph}^*(\lambda)$  is the co-variance with the concentration of chlorophyll a (Chla) [26], and  $S_{dg}$  is specified as  $0.018 \text{ nm}^{-1}$ .

Note that Raman scattering contributes 20% or more to  $R_{rs}(\lambda)$ , especially for wavelengths longer than 550 nm and in oligotrophic waters [44–46]. Therefore, prior to the implementation of QAAv6 and GIOP, an empirical correction of  $R_{rs}(\lambda)$  for the Raman scattering effect was carried out according to the procedure described by Lee et al. [40]. The spectral optimization of GIOP-DC and GSM in general was the same. The codes of the SAAs were all implemented in MATLAB R2017b.

#### 2.4. Quality assurance

We acquired a dataset of coincident observations of  $R_{rs}(\lambda)$ ,  $a_{nw}(\lambda)$ ,  $a_{ph}(\lambda)$  and  $b_{bp}(\lambda)$  from the SCS from 2003 to 2016. Before every cruise, careful calibrations were deployed to correct the drift of the instrument. Data collection in each cruise was conducted by strictly following the NASA Ocean Biology Processing Group defined protocols.

As the  $R_{rs}(\lambda)$  values from in-situ and satellite systems were input to the SAAs to derive the optical and biogeochemical properties of water, and were not error free, an evaluation of the data quality of  $R_{rs}(\lambda)$  is critical. Hence, the quality assurance (QA) system proposed by Wei et al. [48] was used. The QA system contains a scoring system and a classification system. The scoring system provides a score between 0 and 1 to the target  $R_{rs}(\lambda)$  based on a comparison between the target and the reference spectra, where one indicates the highest quality and zero the lowest. Any QA scores in our dataset lower than 0.5 were considered as low quality, and were thus deleted ( $N_{del} = 23$ ) [48]. The codes of the QA system used in the MATLAB script have been made available online at [http://oceanoptics.umb.edu/score\\_metric/](http://oceanoptics.umb.edu/score_metric/).

For IOP data processing, all observations collected below 5 m were discarded, as they were not relevant for this evaluation. All original spectra were visually inspected and data with negative values or questionable shapes were reanalyzed or discarded. Note that quality control was applied to both the in-situ and SAA-retrieved  $a_{ph}(\lambda)$  values based on the International Ocean Color Coordinating Group, which constrained the ratio of  $a_{ph}(412)$  to  $a_{ph}(443)$  to lower than 1.1 and higher than 0.5, and the ratio of  $a_{ph}(490)$  to  $a_{ph}(443)$  to lower than 1 and higher than 0.1. Finally, surface values were calculated by averaging the down-casted data over a depth range of 5 m for all cruises. Specifically, because the measurement bands were not consistent with the bands used in the SAAs, the nearest bands from different instruments for five example wavelengths (412, 443, 490, 531 and 555 nm) that are commonly used in past and current satellite ocean color sensors were selected for the algorithm comparisons.

#### 2.5. Statistical methods

The deviations between the IOPs derived from the SAAs and measurements were calculated to check the consistency of these algorithms. The correlation coefficient (R) provides a measure of the linear correlation between retrievals and measurements and  $R^2$  is the coefficient of determination. The bias, calculated as the average difference between retrievals and measurements, to some extent, provides rough knowledge of the overestimation and underestimation of SAAs. The overall deviation between values derived from the SAAs and measurement was provided by the APD. These statistics are defined as follows:

$$\text{RMSD} = \sqrt{\frac{1}{N} \sum_{n=1}^N ((y_n - \bar{y}) - (x_n - \bar{x}))^2}, \quad (4)$$

$$\sigma_y = \sqrt{\frac{1}{N} \sum_{n=1}^N (y_n - \bar{y})^2}, \quad (5)$$

$$\text{APD} = \frac{1}{N} \sum_{n=1}^N \frac{|y_n - x_n|}{x_n}, \quad (6)$$

where  $y_n$  represents the retrieved value of the model,  $x_n$  represents in-situ values,  $N$  is the number of observations,  $\bar{y}$  is the mean of the model, and  $\bar{x}$  is the mean of the in-situ observations. The Taylor diagram is also used to evaluate the performance of models by displaying a different set of statistics, i.e., centered RMSD (also reference to as unbiased RMSD, uRMSD) and correlation between the model and in-situ data [48].

$$\text{uRMSD} = \sqrt{\sigma_{\text{insitu}}^2 + \sigma_{\text{model}}^2 - 2\sigma_{\text{insitu}}\sigma_{\text{model}}*\Gamma}, \quad (7)$$

On the Taylor diagram used in this paper, these quantities were normalized by the standard deviation ( $\sigma$ ) of the reference, which made it possible to compare different parameters on a single plot. For example, the normalized standard deviation is defined as

$$\sigma^* = \sigma_{\text{model}} / \sigma_{\text{insitu}}. \quad (8)$$

### 3. Results

#### 3.1. Water type class

After quality control, all low-quality data were excluded in this study. The remaining, high-quality dataset was further separated into those of oligotrophic and mesotrophic waters according to the optical water types constrained by  $R_{rs}(\lambda)$ . The QA system provides water class for the target  $R_{rs}(\lambda)$  from 23 reference optical water types, from blue to yellow water. The optical water types of all  $R_{rs}(\lambda)$  spectra are shown in Fig. 3. Note that most of the spectra belonged to 1–4 optical water types (Chla < 0.52 mg m<sup>-3</sup>, N = 173), and the class numbers of few spectra were higher than 10

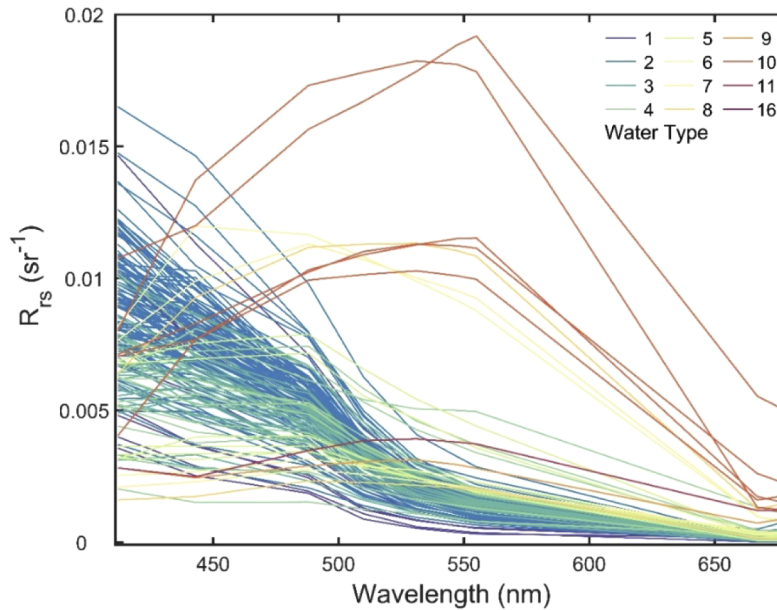


**Fig. 3.** Spectra of  $R_{rs}(\lambda)$  used for SAA evaluation (QA score > 0.5) and optical water type proposed by Wei et al. [47].



( $N = 11$ ). This indicates that most of the water samples in our dataset belonged to relatively clear oceanic water. Here, numbers 1 to 4 of optical type water samples were collected to roughly represent oligotrophic ocean water (Chla between 0.01 to 0.52  $\text{mg m}^{-3}$ ), and the other samples were considered mesotrophic ocean water (Chla between 0.52 to 3.80  $\text{mg m}^{-3}$ ; see Table 1 in Wei et al. [47] for more details).

### 3.2. Comparison of $a_{nw}(\lambda)$ derived from SAAs and measurements

To ensure consistency between the SAA-derived  $a_{nw}(\lambda)$  and in-situ measurements, the values of  $a_w(\lambda)$  from [22] used for field data processing were used in the retrieval of the SAAs. We subsequently compared the in-situ and the SAA-derived  $a_{nw}(\lambda)$  for oligotrophic water samples, mesotrophic water samples, and all samples. Five bands, 412, 443, 490, 531 and 555 nm, consistent with widely used ocean color sensors, were selected for evaluation (Table 2).

**Table 2. Statistics for the QAA and GIOP-DC-derived  $a_{nw}(\lambda)$  at 412, 443, 490, 531 and 555 nm for overall, oligotrophic, and mesotrophic waters. All correlation analyses are significant at  $p < 0.001$ .**

	QAA								
	Entire			Oligotrophic			Mesotrophic		
	APD%	RMSD	$R^2$	APD%	RMSD	$R^2$	APD%	RMSD ( $\text{m}^{-1}$ )	$R^2$
$a_{nw}(412)$	43.88	0.0323	0.77	48.99	0.0311	0.31	15.27	0.0383	0.90
$a_{nw}(443)$	37.93	0.0188	0.84	40.72	0.0189	0.47	13.90	0.0180	0.99
$a_{nw}(490)$	46.97	0.0123	0.85	49.67	0.0122	0.58	23.83	0.0135	0.85
$a_{nw}(531)$	57.57	0.0092	0.74	59.88	0.0089	0.34	37.73	0.0115	0.72
$a_{nw}(555)$	74.88	0.0083	0.74	78.84	0.0081	0.43	40.83	0.0097	0.72
	GIOP-DC								
	Entire			Oligotrophic			Mesotrophic		
	APD%	RMSD	$R^2$	APD%	RMSD	$R^2$	APD%	RMSD ( $\text{m}^{-1}$ )	$R^2$
$a_{nw}(412)$	39.26	0.0283	0.77	43.59	0.0284	0.27	14.98	0.0277	0.92
$a_{nw}(443)$	32.32	0.0164	0.82	34.93	0.0169	0.39	10.91	0.0119	0.97
$a_{nw}(490)$	38.95	0.0111	0.87	42.11	0.0113	0.51	13.04	0.0086	0.95
$a_{nw}(531)$	53.40	0.0085	0.82	57.27	0.0086	0.46	21.57	0.0077	0.90
$a_{nw}(555)$	71.75	0.0085	0.74	76.13	0.0082	0.41	35.76	0.0105	0.81

Similar performance was delivered by the two SAAs. For example, the values of  $R^2$  ranged from 0.74 to 0.85, and 0.74 to 0.87 ( $p < 0.001$ ), and those of the APDs from 37.93% to 74.88%, and from 32.32% to 71.75%, respectively, for the QAA and GIOP-DC. The RMSD values ranged from 0.0083  $\text{m}^{-1}$  to 0.0323  $\text{m}^{-1}$ , and from 0.0085  $\text{m}^{-1}$  to 0.0283  $\text{m}^{-1}$  for the QAA and GIOP-DC, respectively. Further, the retrievals from the SAAs underestimated  $a_{nw}(\lambda)$  relative to their in-situ values, as indicated by the negative biases between them, which ranged from  $-0.0073$  to  $-0.026$   $\text{m}^{-1}$  and from  $-0.0075$  to  $-0.0213$   $\text{m}^{-1}$  for the QAA and GIOP-DC, respectively. If considering two water classes, compared with those for the oligotrophic water samples,  $a_{nw}(\lambda)$  derived from the two SAAs agreed well with the in-situ measurements for mesotrophic water samples. For example, for the mesotrophic water samples, most points are located close to the 1:1 line (Fig. 4, yellow and red circles); this low amount of scatter, and hence good agreement between the algorithm-derived and in-situ measurements, is also demonstrated by the large values of  $R^2$  and small values of the APDs and RMSD (Table 2). However, the oligotrophic water samples presented large differences among all samples (Fig. 4, blue and green circles). In addition, the values of  $R^2$  for the mesotrophic samples ranged from 0.72 to 0.99, and 0.81 to 0.97 for the QAA and GIOP-DC, respectively. In comparison, values of  $R^2$  for the oligotrophic samples were 0.31 to 0.58 and 0.27 to 0.51 for the QAA and GIOP-DC, respectively.

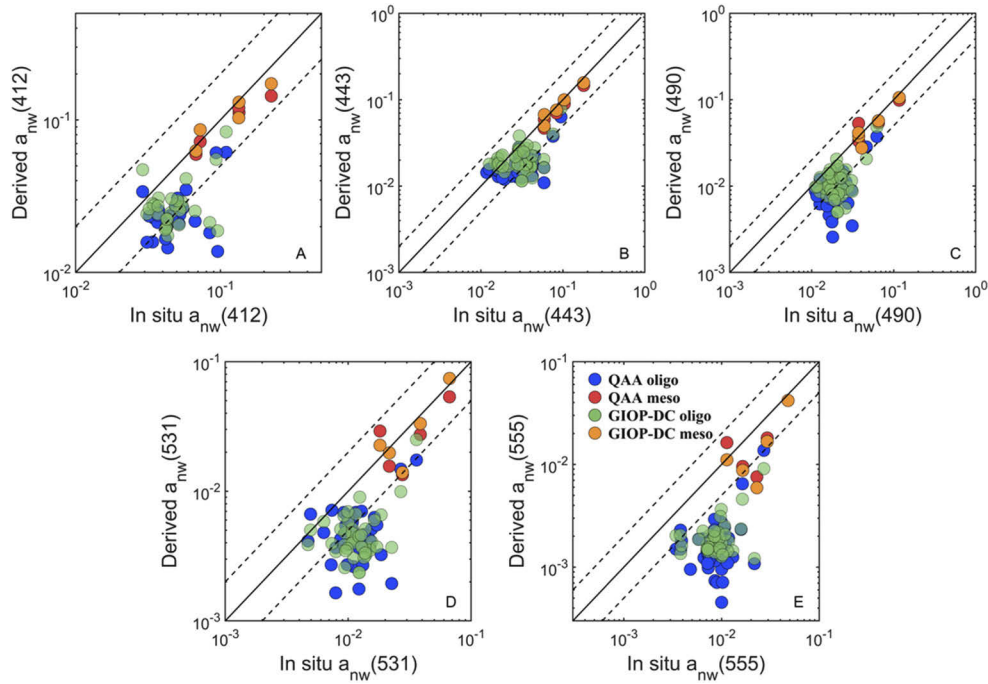


**Fig. 4.** Comparison of retrieved and in-situ-measured  $a_{nw}(\lambda)$  of the QAA and GIOP-DC at 412, 443, 490, 531, and 555 nm for oligotrophic and mesotrophic waters. The black line indicates the 1:1 relationship and the dotted lines represent the 1:1 line  $\pm 30\%$   $\log_{10} a_{nw}(\lambda)$ .

### 3.3. Comparison of the SAA-derived and measured $a_{ph}(\lambda)$

After quality control was applied, 115 match-ups of the SAA-derived and in-situ-measured  $a_{ph}(\lambda)$  values remained, and comparisons were then conducted. Table 3 lists the relevant statistics between the in-situ-measured and SAA-derived  $a_{ph}(\lambda)$  values for all, oligotrophic, and mesotrophic samples (Fig. 5).

The statistics indicate that the QAA-derived  $a_{ph}(\lambda)$  could explain 64% to 91% of the variance of the in-situ  $a_{ph}(\lambda)$ , while the GIOP-DC-derived  $a_{ph}(\lambda)$  explained 76% to 89% of the variance in in-situ  $a_{ph}(\lambda)$  for all samples. Although the GIOP-DC-derived  $a_{ph}(\lambda)$  appeared to better explain the variance of the in-situ  $a_{ph}(\lambda)$  values than the QAA-derived  $a_{ph}(\lambda)$ , greater differences between the in-situ  $a_{ph}(\lambda)$  and the SAA-derived  $a_{ph}(\lambda)$  were seen for all samples, as indicated by the values of APDs ranging from 44.65% to 79.46%, and those of RMSD from 0.0187 to 0.0397  $\text{m}^{-1}$ . The values of the APDs ranged from 43.57% to 83.53% and those of the RMSD from 0.0058 to 0.0157  $\text{m}^{-1}$  for the QAA. Note that the normalized standard deviation of the GIOP-DC-derived  $a_{ph}(\lambda)$  was two times larger than that of the QAA-derived  $a_{ph}(\lambda)$  (1.1 to 2.29 and 2.58 to 5.09 for QAA and GIOP-DC, respectively).

The performance of the two SAAs in terms of estimating  $a_{ph}(\lambda)$  were different between the mesotrophic and oligotrophic samples, as illustrated by the higher values of  $R^2$ , APDs, and RMSE of the former (Table 3). The values of  $R^2$  of the mesotrophic samples ranged from 0.61 to 0.92, and from 0.74 to 0.93 for the QAA and GIOP-DC, respectively. In comparison, the values of  $R^2$  for the oligotrophic samples ranged from 0.21 to 0.36, and from 0.04 to 0.23 for the QAA and GIOP-DC, respectively. Although the  $R^2$  of the mesotrophic samples was higher than that of the oligotrophic samples, it cannot be concluded that the performance of the mesotrophic samples was better than that of the oligotrophic samples because the APDs and RMSE of the

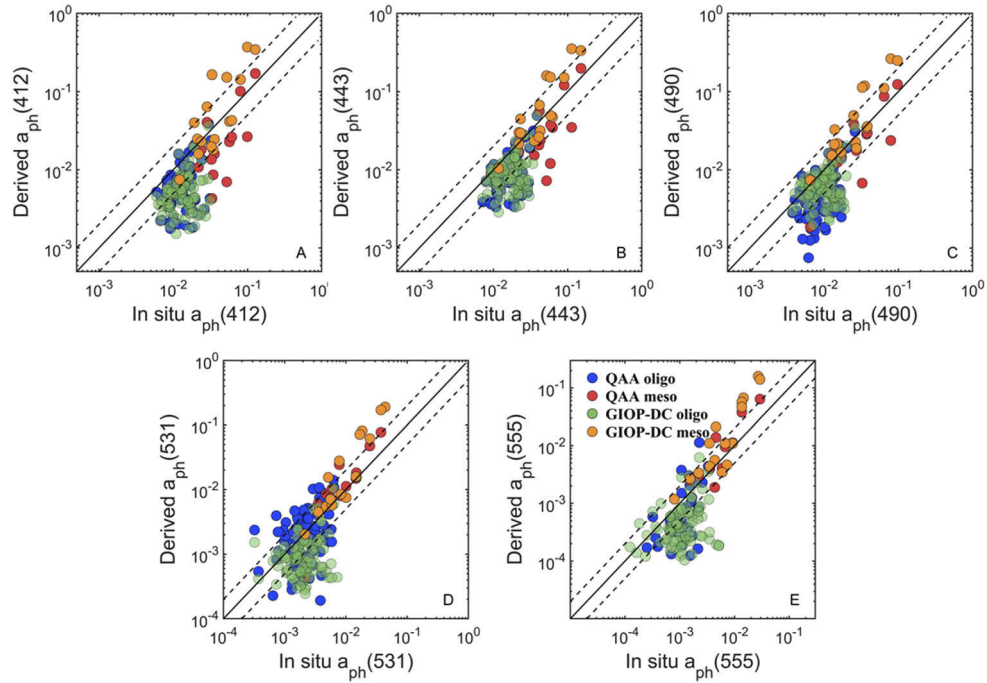


**Fig. 5.** Comparison of retrieved and in-situ-measured  $a_{ph}(\lambda)$  of the QAA and GIOP-DC at 412, 443, 490, 531 and 555 nm for oligotrophic and mesotrophic waters. The black line indicates the 1:1 relationship and the dotted lines represent the 1:1 line  $\pm 30\% \log_{10} a_{ph}(\lambda)$ .

**Table 3.** Statistics for the QAA and GIOP-DC-derived  $a_{ph}(\lambda)$  at 412, 443, 490, 531 and 555 nm for all, oligotrophic, and mesotrophic waters. All correlation analyses are significant at  $p < 0.001$ .

	QAA								
	Entire			Oligotrophic			Mesotrophic		
	APD%	RMSE	$R^2$	APD%	RMSE	$R^2$	APD%	RMSE ( $m^{-1}$ )	$R^2$
$a_{ph}(412)$	51.06	0.0157	0.64	50.12	0.0091	0.21	56.15	0.0335	0.61
$a_{ph}(443)$	43.57	0.0167	0.68	43.08	0.0100	0.29	46.25	0.0352	0.63
$a_{ph}(490)$	43.82	0.0092	0.73	45.19	0.0057	0.36	36.01	0.0197	0.64
$a_{ph}(531)$	83.53	0.0058	0.88	86.57	0.0025	0.21	65.25	0.0142	0.92
$a_{ph}(555)$	70.04	0.0067	0.91	69.32	0.0018	0.27	72.26	0.0131	0.91
	GIOP-DC								
	Entire			Oligotrophic			Mesotrophic		
	APD%	RMSE	$R^2$	APD%	RMSE	$R^2$	APD%	RMSE ( $m^{-1}$ )	$R^2$
$a_{ph}(412)$	63.77	0.0397	0.76	57.14	0.0104	0.15	99.83	0.0979	0.74
$a_{ph}(443)$	46.66	0.0349	0.81	42.22	0.0106	0.20	70.81	0.0851	0.82
$a_{ph}(490)$	44.65	0.0271	0.83	37.16	0.0058	0.23	85.40	0.0675	0.82
$a_{ph}(531)$	67.63	0.0216	0.89	56.14	0.0020	0.17	130.1	0.0547	0.91
$a_{ph}(555)$	79.46	0.0187	0.89	62.38	0.0014	0.04	172.4	0.0474	0.93

mesotrophic samples were higher than those of the oligotrophic samples. For example, the APDs of the mesotrophic samples ranged from 36.01% to 72.26%, and from 70.81% to 172.40% for the QAA and GIOP-DC, respectively. In comparison, the APDs of the oligotrophic samples ranged from 43.08% to 86.57%, and from 37.16% to 62.38% for the QAA and GIOP-DC, respectively. Note that significant negative differences between the SAA-derived  $a_{ph}(\lambda)$  occurred for the oligotrophic samples with negative bias ranging from  $-0.0073$  to  $0.0007 \text{ m}^{-1}$ , and from  $-0.0084$  to  $-0.0007 \text{ m}^{-1}$  for QAA and GIOP-DC, respectively. This negative bias of the oligotrophic samples probably occurred due to the challenging conditions that were present in the relatively clear water when making the measurements of  $a_{ph}(\lambda)$  and the inadequate settings of  $a_{ph}^*(\lambda)$  of the SAAs that lowered the values of  $a_{ph}^*(\lambda)$  compared our in-situ measurements in the SCS.

### 3.4. Comparison of the SAA-derived and measured $b_{bp}(\lambda)$

Only 21 match-ups of  $b_{bp}(\lambda)$  and  $R_{rs}(\lambda)$  from three cruises were used for algorithmic evaluation. The comparative analysis between in-situ-measured  $b_{bp}(\lambda)$  and SAA-derived  $b_{bp}(\lambda)$  was conducted using all, oligotrophic, and mesotrophic samples (Fig. 6 and Table 4).

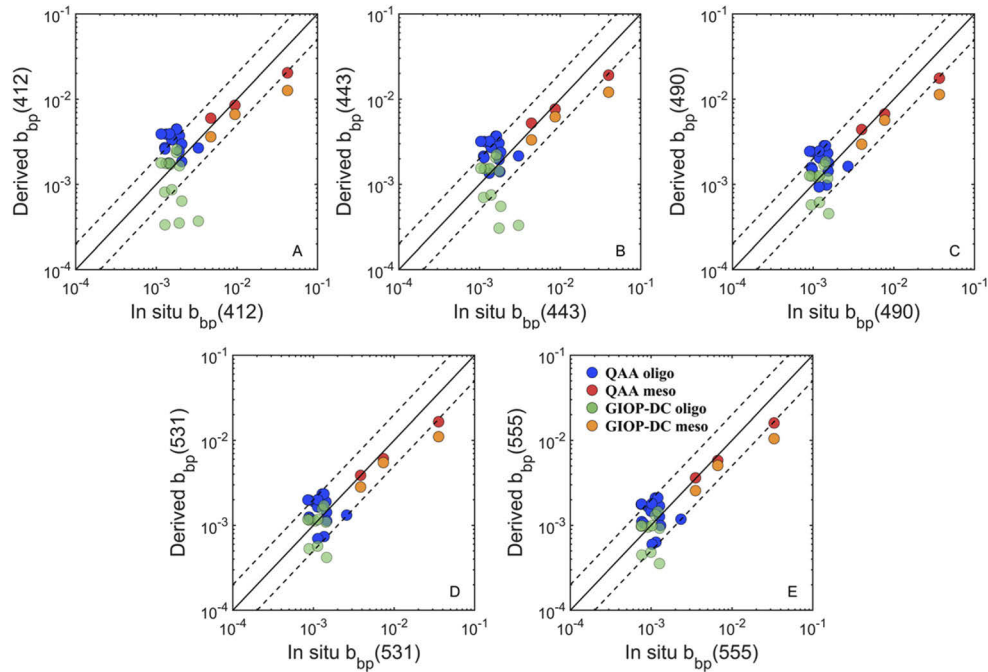


**Fig. 6.** Comparison of retrieved and in-situ-measured  $b_{bp}(\lambda)$  of the QAA and GIOP-DC at 412, 443, 490, 531 and 555 nm for oligotrophic and mesotrophic waters. The black line indicates the 1:1 relationship and dotted lines represent the 1:1 line  $\pm 30\% \log_{10} b_{bp}(\lambda)$ .

The  $b_{bp}(\lambda)$  values derived from the two algorithms exhibited high correlation with the in-situ values for all samples, as indicated by the large values of  $R^2$  exceeding 0.87. The values of APDs ranged from 52.47% to 93.71%, and from 32.08% to 45.88% for all samples for the QAA and GIOP-DC, respectively. In addition, the values of RMSD ranged from 0.0041 to 0.0054  $\text{m}^{-1}$ , and 0.0063 to 0.0075  $\text{m}^{-1}$  for the QAA and GIOP-DC, respectively. If the two types of water were considered separately, prominent deviations from the two SAAs were observed for the oligotrophic samples. For example, retrievals from the QAA that exhibited positive deviations, with bias ranging from 0.0004 to 0.0019  $\text{m}^{-1}$  (Fig. 6, blue circles), while retrievals from the GIOP-DC exhibited negative deviations ranging from  $-0.0005$  to  $-0.0004 \text{ m}^{-1}$  (Fig. 6,

**Table 4. Statistics for the QAA and GIOP-DC-derived  $b_{bp}(\lambda)$  at 412, 443, 490, 531 and 555 nm for all, oligotrophic, and mesotrophic waters. All correlation analyses are significant at  $p < 0.001$ .**

	QAA								
	Entire		Oligotrophic			Mesotrophic			
	APD%	RMSD	$R^2$	APD%	RMSD	$R^2$	APD%	RMSD ( $m^{-1}$ )	$R^2$
$b_{bp}(412)$	93.71	0.0054	0.94	106.58	0.0015	0.04	29.36	0.0127	0.99
$b_{bp}(443)$	79.04	0.0051	0.95	89.36	0.0011	0.03	27.41	0.0120	0.99
$b_{bp}(490)$	65.63	0.0046	0.96	73.75	0.0006	0.03	25.02	0.0111	0.99
$b_{bp}(531)$	52.47	0.0046	0.96	58.21	0.0003	0.02	23.80	0.0110	0.99
$b_{bp}(555)$	53.94	0.0041	0.97	60.25	0.0003	0.02	22.42	0.0100	0.99

	GIOP-DC								
	Entire		Oligotrophic			Mesotrophic			
	APD%	RMSD	$R^2$	APD%	RMSD	$R^2$	APD%	RMSD ( $m^{-1}$ )	$R^2$
$b_{bp}(412)$	45.88	0.0075	0.87	46.99	0.0011	0.09	41.04	0.0172	0.95
$b_{bp}(443)$	42.72	0.0073	0.88	43.19	0.0010	0.18	40.84	0.0161	0.95
$b_{bp}(490)$	33.99	0.0071	0.92	32.04	0.0004	0.01	40.53	0.0147	0.95
$b_{bp}(531)$	33.20	0.0068	0.92	31.04	0.0004	0.01	40.39	0.0142	0.95
$b_{bp}(555)$	32.08	0.0063	0.92	29.66	0.0002	0.02	40.11	0.0132	0.95

green circles). Table 4 indicates that the APDs values of the QAA-derived  $b_{bp}(\lambda)$  were between 58.21% and 106.58% for the oligotrophic samples, while the APDs values were much lower, between 22.42% and 29.36% for the mesotrophic samples. However, differences between the oligotrophic and mesotrophic samples using the GIOP-DC were not as prominent. The APDs values of the GIOP-DC-derived  $b_{bp}(\lambda)$  were between 29.66% and 46.99% for the oligotrophic samples, and between 40.11% and 41.04% for the mesotrophic samples. Note that the differences between the mesotrophic and oligotrophic samples might have occurred due to challenges faced when obtaining the measurements of the IOPs in clear water, as well as the small number of mesotrophic samples, which can yield misleading statistics.

### 3.5. Overall consistency check of the SAAs

In this section, we check the consistency of the SAAs in deriving  $b_{bp}(\lambda)$ ,  $a_{ph}(\lambda)$ , and  $a_{nw}(\lambda)$  for all, oligotrophic, and mesotrophic water samples based on Taylor diagrams. Taylor diagrams (Fig. 7) are used to characterize the skill of a SAA in estimating IOPs in terms of  $R$ , normalized standard deviation, and normalized uRMSD. In the Taylor diagrams, a model performs better if the retrievals are closer to the in-situ points, where in the ideal case,  $r$  is equal to one, normalized uRMSD is zero, and the normalized standard deviation is one.

In terms of the estimated  $a_{nw}(\lambda)$ , the two SAAs performed similarly for all samples and the oligotrophic samples, whereas the GIOP-DC showed small deviations for the mesotrophic samples, as evidenced by the points being closer to the reference point value [Fig. 7(c)]. In general, the deviations of the two SAAs for the mesotrophic samples were smaller than those obtained for the oligotrophic samples, as indicated by their higher  $R$  values, lower uRMSDs, and normalized standard deviations being close to one.

When estimating  $a_{ph}(\lambda)$ , the QAA showed smaller deviations than GIOP-DC for all samples and the mesotrophic samples. As Fig. 7(f) shows, the normalized standard deviations and uRMSDs for  $a_{ph}(\lambda)$  derived by the GIOP-DC were far from the reference points compared with those from the QAA. However, for the oligotrophic samples, the QAA yielded a large normalized standard deviation and uRMSD at 531 nm and 555 nm. Moreover, clear differences in  $a_{ph}(\lambda)$  derived by the QAA and GIOP-DC were found between in the mesotrophic samples



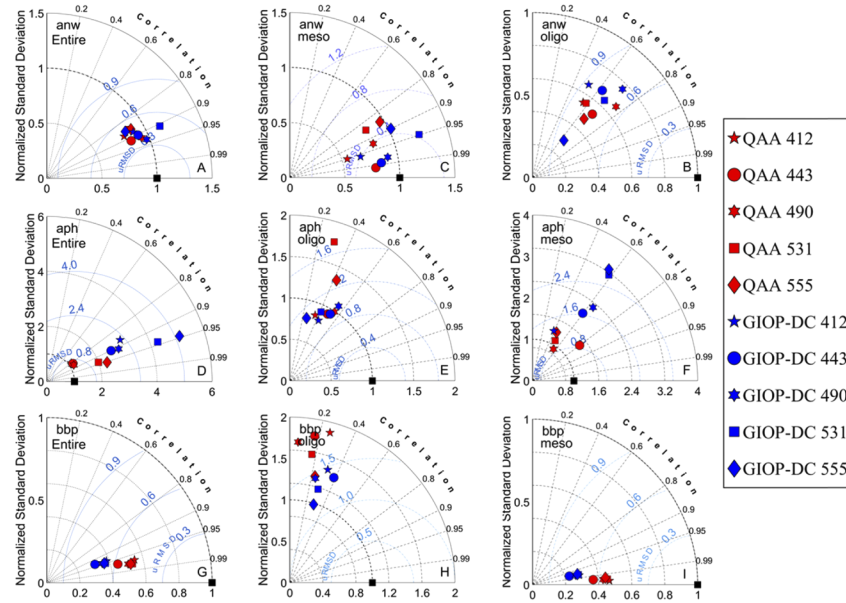


**Fig. 7.** Taylor diagrams illustrating relative model performance of the QAA (red) and GIOP-DC (blue)-derived  $b_{bp}(\lambda)$ ,  $a_{ph}(\lambda)$ , and  $a_{nw}(\lambda)$  for oligotrophic, mesotrophic, and all water samples. The black square represents perfect model performance, where the normalized standard deviation and correlation coefficient are both one.

and oligotrophic samples, where the R values, normalized standard deviation and uRMSD were all higher for the mesotrophic samples.

When estimating  $b_{bp}(\lambda)$ , the QAA-derived  $b_{bp}(\lambda)$  values correlated better with the in-situ measurements than those determined by the GIOP-DC for the mesotrophic samples. However, note that significant differences were observed in the derived  $b_{bp}(\lambda)$  from the QAA for the oligotrophic samples. Compared with the QAA, the GIOP-DC showed higher R and lower uRMSD in oligotrophic waters. In general, the QAA yielded smaller deviations than the GIOP-DC for all samples [Fig. 7(g)]. Similar higher differences between the SAA-derived  $b_{bp}(\lambda)$  and in-situ measurements in oligotrophic waters were also reported by [11]. Both our results here and those of Zheng et al. [11] are associated with the generally lower particulate contribution to total scattering in clear oceanic waters, which leads to errors when estimating  $\eta$ .

#### 4. Discussion

The values of  $a_{nw}(\lambda)$  derived from the two algorithms showed negative differences compared with the in-situ measurements, with biases ranging from  $-0.0073$  to  $-0.026 \text{ m}^{-1}$ , and from  $-0.0075$  to  $-0.0213 \text{ m}^{-1}$  for the QAA and GIOP-DC, respectively. Similar negative differences from the in-situ measurements of the QAA-derived  $a(\lambda)$  were observed by [11] at low latitudes of the eastern South Pacific and eastern Atlantic Oceans. The GIOP-DC obtained  $a_{nw}(\lambda)$  by using the sum of  $a_{ph}(\lambda)$  and  $a_{dg}(\lambda)$ . The sources of differences for the GIOP-DC-derived  $a_{nw}(\lambda)$  originated from the empirical spectral relationships of  $a_{ph}(\lambda)$  and  $a_{dg}(\lambda)$ , and the accuracy of the IOPs- $R_{rs}(\lambda)$  relationship given in Eqs. (1)–(3). Thus, negative differences of  $a_{nw}(\lambda)$  derived by the GIOP-DC occurred owing to the combined effect of  $a_{ph}(\lambda)$  and  $a_{dg}(\lambda)$ .

Moreover, the QAA consisted of two main steps: estimating  $a_{nw}(\lambda)$  and  $b_{bp}(\lambda)$  from  $R_{rs}(\lambda)$  without the need for spectral models of the components, and separating  $a_{nw}(\lambda)$  into  $a_{ph}(\lambda)$  and  $a_{dg}(\lambda)$  (for details, see Fig. 2). The accuracy of the QAA-derived  $a_{nw}(\lambda)$  at the reference

wavelength was only dependent on the accuracy of the empirical relationship between  $a_{nw}(\lambda_0)$  and  $R_{rs}(\lambda)$ , and derivations of  $a_{nw}(\lambda)$  at non-reference wavelengths were influenced by both the accuracy of the estimated  $\eta$  and the IOPs– $R_{rs}(\lambda)$  relationship [49] [Eqs. (1)–(3) here] given by Gordon et al. [37]. The effect of  $\eta$  on the accuracy of the QAA-derived  $a_{nw}(\lambda)$  was minor for the range between 490 nm and 670 nm but tended to increase at wavelengths shorter than 443 nm [11]. These conclusions are consistent with our statistical results, whereby the highest bias values appeared at 412 nm ( $-0.026 \text{ m}^{-1}$ ). Moreover, SAAs require a forward model to link the IOPs to  $R_{rs}(\lambda)$ , but different IOPs– $R_{rs}(\lambda)$  relationships can have different effects on the computed  $R_{rs}(\lambda)$ , which influenced the accuracies of the derived IOPs [49]. In particular, Mason et al. [22] showed that  $a_w(\lambda)$  used by Pop and Fry et al. [43] had errors, which they corrected for and improved their measurements. Moreover, Lee et al. [50] obtained  $a_w(\lambda)$  from remote sensing reflectance in oligotrophic oceans based on “pure” seawater. However, these three  $a_w(\lambda)$  derivations all had large deviations at shorter wavelengths ( $< 450 \text{ nm}$ ). These differences in the three  $a_w(\lambda)$  might have induced errors directly when obtaining IOPs from SAAs in oligotrophic waters, especially for  $a_{ph}(\lambda)$  at shorter wavelengths [51].

The QAA-derived  $a_{ph}(\lambda)$  correlated relatively well and showed smaller differences with the in-situ  $a_{ph}(\lambda)$  for all samples, while the performances of the QAA-derived  $a_{ph}(\lambda)$  at 531 and 555 nm were unsatisfactory for the oligotrophic samples. This might be because the QAA decomposed the  $a_{nw}(\lambda)$  into  $a_{ph}(\lambda)$  and  $a_{dg}(\lambda)$ , which were depending on bio-optical models based on some assumptions. This might have introduced uncertainties into the retrievals of  $a_{ph}(\lambda)$  and  $a_{dg}(\lambda)$ . Notably, all uncertainties, including those due to errors in  $R_{rs}(\lambda)$  and  $a_{dg}(\lambda)$ , were propagated to  $a_{ph}(\lambda)$  because the QAA calculated  $a_{ph}(\lambda)$  by the difference between  $a_{nw}(\lambda)$  and  $a_{dg}(\lambda)$ . This might be the other reason for the large deviation in  $a_{ph}(\lambda)$  derived from the QAA. More accurate bio-optical assumptions, and empirical methods of the estimation of  $a(\lambda_0)$ , spectral power  $\eta$ , spectral slope  $S$ , and the ratio of  $a_{ph}(412)/a_{ph}(443)$  are necessary for the QAA to improve its accuracy of retrieval of  $a_{ph}(\lambda)$ . Clear negative differences in  $a_{ph}(\lambda)$  in the oligotrophic samples and large standard normalized deviations in the mesotrophic samples appeared for the GIOP-DC in our SCS dataset. Similar situations have been observed in the Northern Gulf of California [52], Korea’s coastal waters [13], the coastal Yellow Sea, and in the East China Sea [12]. The GIOP-DC applied power law functions to express  $a_{ph}(\lambda)$  as a function of Chla [26,27,53]. The negative deviations of the GIOP-DC-derived  $a_{ph}(\lambda)$  (Fig. 5 and Fig. 7) might have obtained owing to improper settings of  $a_{ph}^*(\lambda)$  [54]. However, such settings designed for global waters have limitations when applied to the SCS. Thus, we analyzed the in-situ-measured  $a_{ph}(\lambda)$  in our datasets, tuned the values of  $a_{ph}^*(\lambda)$  for the GIOP-DC, and attempted to improve the estimation of  $a_{ph}(\lambda)$ .

In short, the GIOP-DC set  $a_{ph}^*(\lambda)$  as a function of Chla according to Bricaud et al. [26] and normalized  $a_{ph}^*(443) = 0.055 \text{ m}^2 \text{ mg}^{-1}$ . However, in our SCS dataset, the mean value of  $a_{ph}^*(443)$  of the in-situ measurements was  $0.1176 \text{ m}^2 \text{ mg}^{-1}$  [Fig. 8(A), dotted line], consistent with a previous study in this area with a proposal for  $a_{ph}^*(443)$  of 0.137 proposed by Wang et al. [55]. The mean values of  $a_{ph}^*(\lambda)$  at the six wavelengths were 0.0997, 0.1176, 0.0781, 0.0274, 0.0169, and  $0.0489 \text{ m}^2 \text{ mg}^{-1}$ , respectively. There was a linear relationship between the GIOP-DC-derived Chla and the in-situ Chla, which accounted for 73% of the variance in the in-situ Chla (Fig. 9,  $F(1,89) = 368.3$ ,  $p < 0.001$ ,  $R^2 = 0.73$ , linear regression). Moreover, few negative differences were exhibited by the GIOP-DC-derived Chla values, as indicated by a negative bias of ( $-0.01 \text{ mg m}^{-3}$ ). The predicted  $a_{ph}(\lambda)$  was the product of Chla and  $a_{ph}^*(\lambda)$ . Therefore, negative differences in the GIOP-DC-derived  $a_{ph}(\lambda)$  might have occurred because of lower values of  $a_{ph}^*(\lambda)$  used in the GIOP-DC than the in-situ values in the SCS.

The reasons for the high  $a_{ph}^*(443)$  values of our SCS dataset relative to the values found by Bricaud et al. [26] were probably due to (1) different methods of path-length amplification factor corrections in the calculations of  $a_{ph}(\lambda)$  and (2) different measurement methods of Chla. In

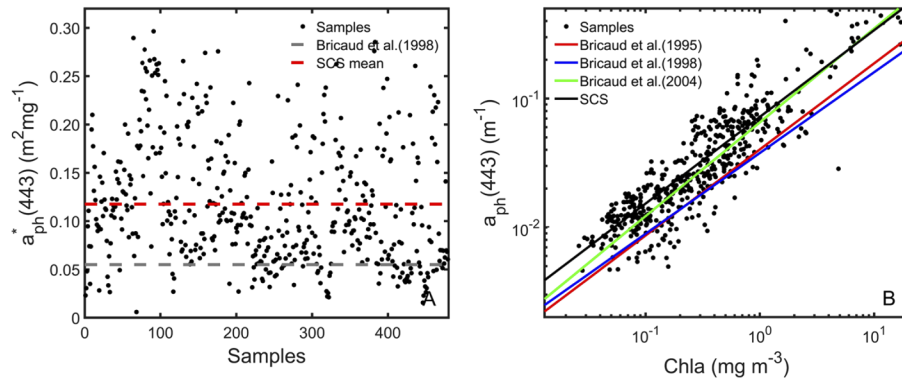


**Fig. 8.** (a) Values of  $a_{ph}^*(443)$  for all samples in the SCS dataset. The dotted red line represents the mean value of  $a_{ph}^*(443)$  ( $0.1176 \text{ m}^2 \text{ mg}^{-1}$ ) and the gray dotted line represents the mean value ( $0.055 \text{ m}^2 \text{ mg}^{-1}$ ) reported by Bricaud et al. (1998). (b) Scatter plots of Chla and  $a_{ph}(443)$  in the SCS dataset.

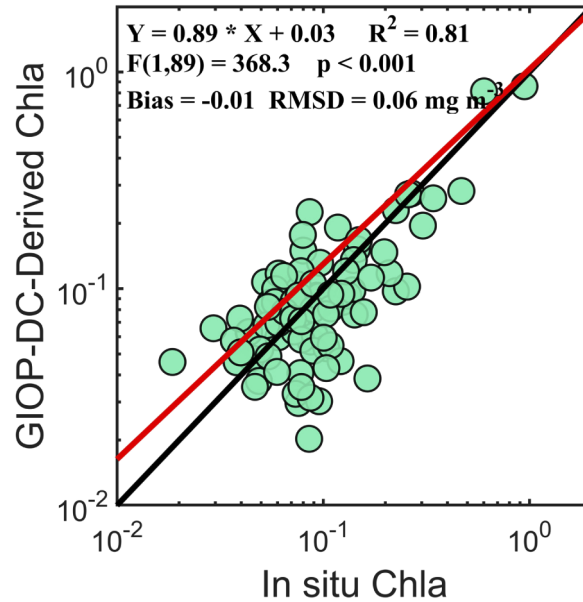


**Fig. 9.** Comparison between the GIOP-DC-derived Chla and in-situ Chla. The red line represents the GIOP-DC-fitted line.

the calculation of  $a_{ph}(\lambda)$ , the path-length amplification factor correction method of Stramski et al. [28] was adopted in our study. The  $a_{ph}(\lambda)$  values of the SCS dataset were also recalculated using the method of Bricaud et al. [26]. The comparison of two different  $a_{ph}(\lambda)$  datasets show that the mean  $a_{ph}(443)$  derived using the values of Stramski et al. [28] was significantly higher (APD = 12.95%) than that derived by Bricaud et al. [26] (one-way ANOVA,  $F = 16.05$ ,  $p < 0.001$ , bias  $> 0$ ,  $N = 872$ ). Moreover, our Chla dataset was measured by high performance liquid chromatography, while the Chla values used in Bricaud et al. [26] were mainly measured by fluorometry. Although the different methods showed relatively well consistence [56], these differences cannot be ignored especially at low Chla values [57–59]. Meanwhile, Bricaud and collaborators also showed a new relationship between  $a_{ph}(440)$  and Chla [53], which is similar

to the relationship found here [Fig. 8(b)]. Moreover, almost 60% higher  $a_{ph}(440)$  values were observed at the same Chla level compared to the older results of Bricaud et al. [26]; hence we attribute the higher values of  $a_{ph}(443)$  found here to the different Chla measurement methods.

To overcome the effects of these deviations, the constants A and B of the GIOP-DC in Bricaud et al. [26] were retuned on the SCS dataset ( $A = [0.064, 0.072, 0.048, 0.024, 0.016, 0.045]$  and  $B = [0.296, 0.326, 0.325, 0.108, 0.061, 0.069]$ ,  $N = 479$ ). Once A and B had been confirmed,  $a_{ph}^*(443)$  was normalized to 0.1176. Figure 10 illustrates clear improvements in the tuned GIOP as the scatter now exists closer to the 1:1 line; reduced scatter is also indicated by the RMSD values decreasing from 0.0187–0.0397 to 0.0049–0.0168  $\text{mg m}^{-3}$ . Further, in the case where there was no significant difference between the means of the GIOP-DC-derived  $a_{ph}(\lambda)$  and the tuned GIOP-derived  $a_{ph}(\lambda)$  (one-way ANOVA,  $p = 0.76$ ,  $p = 0.68$ ,  $p = 0.58$ ,  $p = 0.51$ , and  $p = 0.36$  for 412, 443, 490, 531, and 555 nm, respectively), the normalized standard deviations decreased nearly by half (Table 5). The negative differences in the GIOP-DC-derived  $a_{ph}(\lambda)$  for low values were thus overcome. These results suggest that the GIOP, when tuned to match the optical properties of local phytoplankton, can perform better than a universal algorithm applied indiscriminately to a local ocean. Note that we are not seeking a precise improved method to estimate  $a_{ph}(\lambda)$ , but suggest that optional values of  $a_{ph}^*(\lambda)$  for different water samples might improve the estimated  $a_{ph}(\lambda)$ .

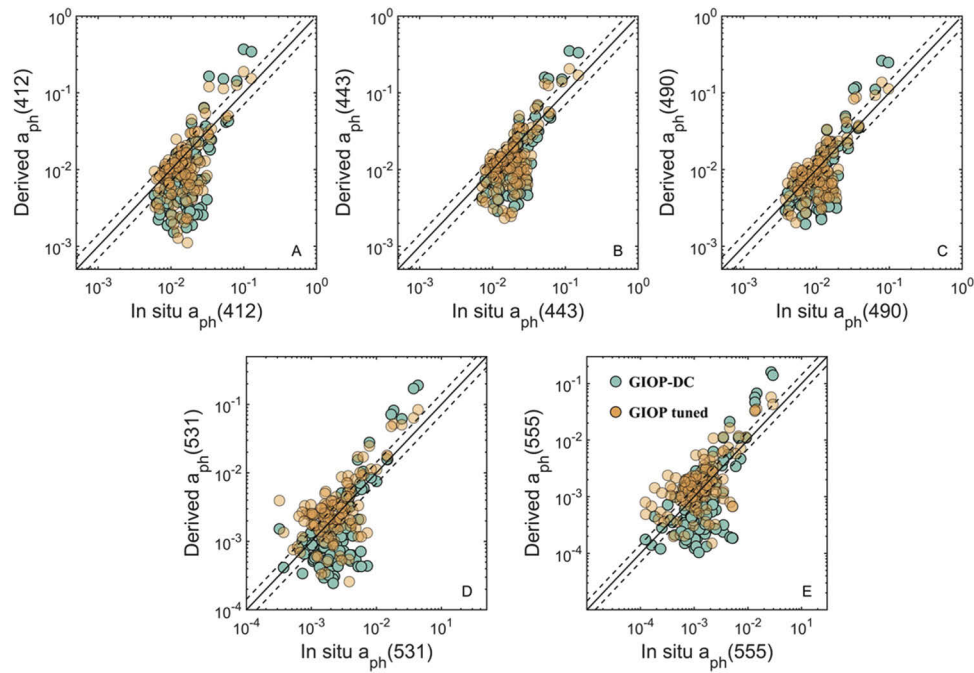


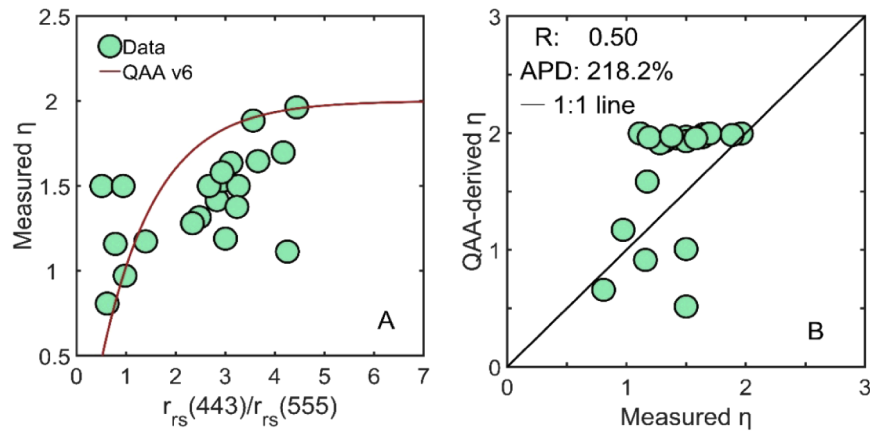
**Fig. 10.** Comparison among the GIOP-DC, and tuned GIOP-derived  $a_{ph}(\lambda)$  and in-situ  $a_{ph}(\lambda)$ . The black line indicates the 1:1 relationship and dotted lines represent the 1:1 line  $\pm 30\% \log_{10} a_{ph}(\lambda)$ .

There were two main sources of uncertainties in estimating  $b_{bp}(\lambda)$ : that in the estimation of  $b_{bp}(\lambda_0)$  and that in the spectral power  $\eta$ . For the QAA system, the uncertainty in  $b_{bp}(\lambda_0)$  was proportional to that in  $a(\lambda_0)$ , but uncertainties in the values at other wavelengths depended on the accuracy of  $\eta$ . Lee et al. [39] have indicated that when both  $a(\lambda_0)$  and  $\eta$  are error free, the derived  $b_{bp}(\lambda)$  at other wavelengths is also error free. Both QAA and GIOP-DC estimated  $\eta$  from  $R_{rs}(\lambda)$ . In practice,  $\eta$  likely varied between zero and three in oceans based on the characteristics of the

**Table 5. Statistics for the GIOP-DC, and tuned GIOP-derived  $a_{ph}(\lambda)$  at 412, 443, 490, 531 and 555 nm. All correlation analyses are significant at  $p < 0.001$ .**

	GIOP-DC			Tuned GIOP		
	APD%	RMSD ( $m^{-1}$ )	Normalized SD	APD%	RMSD ( $m^{-1}$ )	Normalized SD
$a_{ph}(412)$	63.77	0.0397	3.05	35.04	0.0163	1.69
$a_{ph}(443)$	46.66	0.0349	2.58	33.69	0.0168	1.62
$a_{ph}(490)$	44.65	0.0271	2.86	33.58	0.0110	1.60
$a_{ph}(531)$	67.63	0.0216	4.27	58.10	0.0071	2.02
$a_{ph}(555)$	79.46	0.0187	5.09	75.37	0.0049	1.98

constituents of the water [60]. In some inverse models, the value of  $\eta$  was parameterized to 0.5 in coastal waters and to one for oceanic waters [61]. In our study, the mean value of the in-situ fitted  $\eta$  was about 1.42. The empirically derived values of  $\eta$  for the QAA and GIOP-DC were higher than the setting for oceanic water in general, with APD about 218.2% (Fig. 11). This finding is consistent with the results reported by Zheng et al. [11] which showed the QAA-derived  $\eta$  exhibited relatively high correlation with values derived from measurements of Arctic data, but correlated poorly with measurements at lower latitudes collected mostly in clear water. Because the estimation of  $\eta$  features large uncertainty, many empirical methods have been proposed to address this issue [10]. The estimation of  $\eta$  was improved, with a higher R of 0.75, by applying a backscattering coefficient at a fixed wavelength [10]. In addition, the QAA-derived  $b_{bp}(\lambda)$  for oligotrophic water showed positive deviations as indicated by the positive bias. By comparison, GIOP-DC-derived  $b_{bp}(\lambda)$  for oligotrophic water showed negative differences from the in-situ  $b_{bp}(\lambda)$ . Zheng et al. [11] noted that overestimations of the QAA-derived  $b_{bp}(\lambda)$  for oligotrophic water occurred mostly because of the contribution to Raman scattering, which can enhance reflectance by at least 15% in the green and red spectra, and can lead to the overestimation of the QAA-derived  $b_{bp}(\lambda)$ . As our results show, the QAA-derived  $b_{bp}(\lambda)$  without Raman correction showed positive differences, and had biases as high as 0.0004 to 0.0027  $m^{-1}$  compared with those that were Raman-corrected, whose biases were 0.0004 to 0.0019  $m^{-1}$ . As the GIOP-DC used the same approach as the QAA to derive  $\eta$ , the opposing performance of the QAA- and GIOP-DC-derived  $b_{bp}(\lambda)$  on oligotrophic water occurred mainly due to the accuracy of the calculated  $b_{bp}(\lambda_0)$ . Although there was error in the estimation of  $\eta$ , this parameter had a smaller

**Fig. 11.** (a) Comparison of function of QAA\_v6 with that derive  $\eta$  from  $r_{rs}(443)/r_{rs}(555)$ , and (b) QAA\_v6-derived  $\eta$  and in-situ-measured  $\eta$ .



influence on  $b_{bp}(\lambda)$  than  $b_{bp}(\lambda_0)$ . For example,  $\eta$  was overestimated by 50% if its real value was one, and  $b_{bp}(412)$  was overestimated by about 15%. Therefore, it was important to correct for Raman scattering and implement the refined parameterization of the IOPs– $R_{rs}(\lambda)$  relationship for oligotrophic water [40].

## 5. Conclusions

The fundamental difficulty in checking the consistency of SAAs in the SCS is a lack of reliable and sufficient concurrent in-situ match-ups of data from the AOPs and IOPs. To overcome this difficulty, a large dataset containing in-situ values of  $a_{ph}(\lambda)$ ,  $a_{nw}(\lambda)$ ,  $b_{bp}(\lambda)$ , and the corresponding  $R_{rs}(\lambda)$  were gathered in the SCS, covering coastal to extreme clear oceanic waters from 2003 to 2016. After quality control by the QA system, a total of 194 match-ups of  $a_{ph}(\lambda)$ , 56 match-ups of  $a_{nw}(\lambda)$ , and 21 match-ups of  $b_{bp}(\lambda)$  and the concurrent  $R_{rs}(\lambda)$  were used to provide a credible consistency check between the SAA-derived IOPs and in-situ measurements in the SCS. The water samples were separated into oligotrophic and mesotrophic waters for comparison based on the optical water types proposed by Wei et al. [44]. In addition, a better way of approaching the estimation of  $a_{ph}(\lambda)$  was provided and analyzed.

Our study led to several findings: (1) No prominent differences were evident for the two SAA-derived  $a_{nw}(\lambda)$  over all samples, and the GIOP-DC-derived  $a_{nw}(\lambda)$  yielded small differences relative to the in-situ  $a_{nw}(\lambda)$  for the mesotrophic samples; (2) Negative differences between the SAA-derived  $a_{ph}(\lambda)$  and in-situ  $a_{ph}(\lambda)$  were evident in the oligotrophic samples, and thus an accurate  $a_{ph}^*(\lambda)$  was needed. The QAA-derived  $a_{ph}(\lambda)$  showed relatively smaller differences relative to the in-situ  $a_{ph}(\lambda)$  than those of the GIOP-DC-derived  $a_{ph}(\lambda)$  for all samples, and no prominent differences between the two SAA-derived  $a_{ph}(\lambda)$  with the in-situ  $a_{ph}(\lambda)$  were found for the oligotrophic samples. (3) The QAA-derived  $b_{bp}(\lambda)$  showed smaller deviations with the in-situ  $b_{bp}(\lambda)$  than GIOP-DC for all samples, while the GIOP-DC-derived  $b_{bp}(\lambda)$  were closer to the in-situ measurements than the QAA-derived values for the oligotrophic samples.

## Funding

Key Special Project for Introduced Talents Team of Southern Marine Science and Engineering Guangdong Laboratory (Guangzhou) (GML2019ZD0305, GML2019ZD0602); National Natural Science Foundation of China (41976172, 41976170, 41576030, 41976181, 41776044, 41776045, 41606199); Guangzhou Municipal Science and Technology Project (201707020023).

## Acknowledgments

We thank our colleagues in the Optics Laboratory at the South China Sea Institute of Oceanology, Chinese Academy of Sciences, who contributed to the collection and processing of the field data used in this study. We also thank the National Natural Science Foundation of China for its field campaigns.

## Disclosures

The authors declare no conflicts of interest.

## References

1. IOCCG, "Why Ocean Colour? The Societal Benefits of OceanColour Technology," in *Reports of International Ocean-Colour Coordinating Group*, Trevor Platt, ed. (IOCCG, 2008).
2. P. J. Werdell, B. A. Franz, S. W. Bailey, G. C. Feldman, E. Boss, V. E. Brando, M. Dowell, T. Hirata, S. J. Lavender, Z. Lee, H. Loisel, S. Maritorena, F. Melin, T. S. Moore, T. J. Smyth, D. Antoine, E. Devred, O. H. F. d'Andon, and A. Mangin, "Generalized ocean color inversion model for retrieving marine inherent optical properties," *Appl. Opt.* **52**(10), 2019–2037 (2013).

3. R. J. W. Brewin, S. Sathyendranath, D. Müller, C. Brockmann, P.-Y. Deschamps, E. Devred, R. Doerffer, N. Fomferra, B. Franz, M. Grant, S. Groom, A. Horseman, C. Hu, H. Krasemann, Z. Lee, S. Maritorena, F. Mélin, M. Peters, T. Platt, P. Regner, T. Smyth, F. Steinmetz, J. Swinton, J. Werdell, and G. N. White, "The Ocean Colour Climate Change Initiative: III. A round-robin comparison on in-water bio-optical algorithms," *Remote Sens. Environ.* **162**, 271–294 (2015).
4. E. Devred, S. Sathyendranath, V. Stuart, H. Maass, O. Ulloa, and T. Platt, "A two-component model of phytoplankton absorption in the open ocean: Theory and applications," *J. Geophys. Res.* **111**(C3), C03011 (2006).
5. S. A. Garver and D. A. Siegel, "Inherent optical property inversion of ocean color spectra and its biogeochemical interpretation .I. Time series from the Sargasso Sea," *J. Geophys. Res.: Oceans* **102**(C8), 18607–18625 (1997).
6. F. E. Hoge and P. E. Lyon, "Satellite retrieval of inherent optical properties by linear matrix inversion of oceanic radiance models: An analysis of model and radiance measurement errors," *J. Geophys. Res.: Oceans* **101**(C7), 16631–16648 (1996).
7. M. Kisino, M. Takahashi, N. Okami, and S. Ichimura, "Estimation of the spectral absorption coefficients of phytoplankton in the sea," *Bull. Mar. Sci.* **37**, 634–642 (1985).
8. Z. P. Lee, K. L. Carder, and R. A. Arnone, "Deriving inherent optical properties from water color: a multiband quasi-analytical algorithm for optically deep waters," *Appl. Opt.* **41**(27), 5755–5772 (2002).
9. S. Maritorena, D. A. Siegel, and A. R. Peterson, "Optimization of a semianalytical ocean color model for global-scale applications," *Appl. Opt.* **41**(15), 2705–2714 (2002).
10. S. G. Chen and T. L. Zhang, "Evaluation of a QAA-based algorithm using MODIS land bands data for retrieval of IOPs in the Eastern China Seas," *Opt. Express* **23**(11), 13953–13971 (2015).
11. G. M. Zheng, D. Stramski, and R. A. Reynolds, "Evaluation of the Quasi-Analytical Algorithm for estimating the inherent optical properties of seawater from ocean color: Comparison of Arctic and lower-latitude waters," *Remote Sens. Environ.* **155**, 194–209 (2014).
12. J. Huang, L. Q. Chen, X. L. Chen, and Q. J. Song, "Validation of semi-analytical inversion models for inherent optical properties from ocean color in coastal Yellow Sea and East China Sea," *J. Oceanogr.* **69**(6), 713–725 (2013).
13. P. Shanmugam, Y.-H. Ahn, J.-H. Ryu, and B. Sundarabalan, "An evaluation of inversion models for retrieval of inherent optical properties from ocean color in coastal and open sea waters around Korea," *J. Oceanogr.* **66**(6), 815–830 (2010).
14. M. H. Dai, W. D. Zhai, W. J. Cai, J. Callahan, B. Huang, S. L. Shang, T. Huang, X. L. Li, Z. M. Lu, W. F. Chen, and Z. Z. Chen, "Effects of an estuarine plume-associated bloom on the carbonate system in the lower reaches of the Pearl River estuary and the coastal zone of the northern South China Sea," *Cont. Shelf Res.* **28**(12), 1416–1423 (2008).
15. S. L. Shang, L. Li, F. Q. Sun, J. Y. Wu, C. M. Hu, D. W. Chen, X. R. Ning, Y. Qiu, C. Y. Zhang, and S. P. Shang, "Changes of temperature and bio-optical properties in the South China Sea in response to Typhoon Lingling, 2001," *Geophys. Res. Lett.* **35**(10), 1–6 (2008).
16. L. Deng, W. Zhou, W. X. Cao, W. D. Zheng, G. F. Wang, Z. T. Xu, C. Li, Y. Y. Yang, S. B. Hu, and W. J. Zhao, "Retrieving Phytoplankton Size Class from the Absorption Coefficient and Chlorophyll A Concentration Based on Support Vector Machine," *Remote Sens.* **11**(9), 1054 (2019).
17. S. B. Hu, W. Zhou, G. F. Wang, W. X. Cao, Z. T. Xu, H. Z. Liu, G. F. Wu, and W. J. Zhao, "Comparison of Satellite-Derived Phytoplankton Size Classes Using In-Situ Measurements in the South China Sea," *Remote Sens.* **10**(4), 526 (2018).
18. J. F. Lin, W. X. Cao, G. F. Wang, W. Zhou, Z. H. Sun, and W. J. Zhao, "Inversion of bio-optical properties in the coastal upwelling waters of the northern South China Sea," *Cont. Shelf Res.* **85**, 73–84 (2014).
19. J. L. Mueller, A. Morel, R. Frouin, C. Davis, R. Arnone, and K. Carder, "Radiometric Measurements and Data Analysis Protocols, Revision 4," N. T. Memorandum, ed. (NASA Goddard Space Center, Greenbelt, Maryland, 2003), pp. 1–78.
20. D. A. Toole, D. A. Siegel, D. W. Menzies, M. J. Neumann, and R. C. Smith, "Remote-sensing reflectance determinations in the coastal ocean environment: impact of instrumental characteristics and environmental variability," *Appl. Opt.* **39**(3), 456–469 (2000).
21. G. Zibordi, S. B. Hooker, J. F. Berthon, and D. D'Alimonte, "Autonomous above-water radiance measurements from an offshore platform: A field assessment experiment," *J. Atmos. Oceanic Technol.* **19**(5), 808–819 (2002).
22. J. D. Mason, M. T. Cone, and E. S. Fry, "Ultraviolet (250–550 nm) absorption spectrum of pure water," *Appl. Opt.* **55**(25), 7163–7172 (2016).
23. X. Zhang, L. Hu, and M.-X. He, "Scattering by pure seawater: Effect of salinity," *Opt. Express* **17**(7), 5698–5710 (2009).
24. B. G. Mitchell, "Algorithms for determining the absorption coefficient of aquatic particulates using the quantitative filter technique(QFT)," *Proc. SPIE* **1302**, 137–148 (1990).
25. C. S. Yentsch, "Measurement of visible light absorption by particulate matter in the ocean," *Limnol. Oceanogr.* **7**(2), 207–217 (1962).
26. A. Bricaud, M. Babin, A. Morel, and H. Claustre, "Variability in the chlorophyll-specific absorption coefficients of natural phytoplankton: Analysis and parameterization," *J. Geophys. Res.* **100**(C7), 13321 (1995).
27. A. Bricaud, A. Morel, M. Babin, K. Allali, and H. Claustre, "Variations of light absorption by suspended particles with chlorophylla concentration in oceanic (case 1) waters: Analysis and implications for bio-optical models," *J. Geophys. Res.* **103**(C13), 31033–31044 (1998).

28. D. Stramski, R. A. Reynolds, S. Kaczmarek, J. Uitz, and G. Zheng, "Correction of pathlength amplification in the filter-pad technique for measurements of particulate absorption coefficient in the visible spectral region," *Appl. Opt.* **54**(22), 6763–6782 (2015).
29. J. F. Lin, W. X. Cao, G. F. Wang, and S. B. Hu, "Satellite-observed variability of phytoplankton size classes associated with a cold eddy in the South China Sea," *Mar. Pollut. Bull.* **83**(1), 190–197 (2014).
30. G. F. Wang, W. X. Cao, D. T. Yang, and J. Zhao, "Partitioning particulate absorption coefficient into contributions of phytoplankton and nonalgal particles: A case study in the northern South China Sea," *Estuarine, Coastal Shelf Sci.* **78**(3), 513–520 (2008).
31. C. S. Roesler and A. H. Barnard, "Optical proxy for phytoplankton biomass in the absence of photophysiology: Rethinking the absorption line height," *Methods in Oceanogr.* **7**, 79–94 (2013).
32. J. Sullivan, M. Twardowski, J. R. V. Zaneveld, C. Moore, A. H. Barnard, P. L. Donaghay, and B. Rhoades, "Hyperspectral temperature and salt dependencies of absorption by water and heavy water in the 400–750nm spectral range," *Appl. Opt.* **45**(21), 5294–5309 (2006).
33. D. McKee, J. Piskozub, and I. Brown, "Scattering error corrections for in situ absorption and attenuation measurements," *Opt. Express* **16**(24), 19480–19492 (2008).
34. D. McKee, J. Piskozub, R. Roettgers, and R. A. Reynolds, "Evaluation and Improvement of an Iterative Scattering Correction Scheme for in situ Absorption and Attenuation Measurements," *J. Atmos. Oceanic Technol.* **30**(7), 1527–1541 (2013).
35. J. R. V. Zaneveld, J. C. Kitchen, and C. C. Moore, "Scattering error correction of reflecting-tube absorption meters," *Proc. SPIE* **2258**, 44–55 (1994).
36. R. A. Maffione and D. R. Dana, "Instruments and methods for measuring the backward-scattering coefficient of ocean waters," *Appl. Opt.* **36**(24), 6057–6067 (1997).
37. P. J. Werdell, L. I. W. McKinna, E. Boss, S. G. Ackleson, S. E. Craig, W. W. Gregg, Z. Lee, S. Maritorena, C. S. Roesler, C. S. Rousseaux, D. Stramski, J. M. Sullivan, M. S. Twardowski, M. Tzortziou, and X. Zhang, "An overview of approaches and challenges for retrieving marine inherent optical properties from ocean color remote sensing," *Prog. Oceanogr.* **160**, 186–212 (2018).
38. H. R. Gordon, O. B. Brown, R. H. Evans, J. W. Brown, R. C. Smith, K. S. Baker, and D. K. Clark, "A semianalytic radiance model of ocean color," *J. Geophys. Res.* **93**(D9), 10909–10924 (1988).
39. Z. P. Lee, R. Arnone, C. M. Hu, P. J. Werdell, and B. Lubac, "Uncertainties of optical parameters and their propagations in an analytical ocean color inversion algorithm," *Appl. Opt.* **49**(3), 369–381 (2010).
40. Z. P. Lee, C. M. Hu, S. L. Shang, K. P. Du, M. Lewis, R. Arnone, and R. Brewin, "Penetration of UV-visible solar radiation in the global oceans: Insights from ocean color remote sensing," *J. Geophys. Res.: Oceans* **118**(9), 4241–4255 (2013).
41. Z. P. Lee, A. Weidemann, J. Kindle, R. Arnone, K. L. Carder, and C. Davis, "Euphotic zone depth: Its derivation and implication to ocean-color remote sensing," *J. Geophys. Res.* **112**, C3–C11 (2007).
42. Z. P. Lee, B. Lubac, P. J. Werdell, and R. Arnone, "An update of the quasi-analytical algorithm (QAA\_v5)," in *Reports of International Ocean-Colour Coordinating Group*, Mark Dowell and Trevor Platt, eds. (IOCCG, 2009).
43. R. M. Pope and E. S. Fry, "Absorption spectrum (380–700 nm) of pure water. 2. Integrating cavity measurements," *Appl. Opt.* **36**(33), 8710–8723 (1997).
44. R. H. Stavn and A. D. Weidemann, "Optical modeling of clear ocean light fields - Raman scattering effects," *Appl. Opt.* **27**(19), 4002–4011 (1988).
45. A. Morel, D. Antoine, and B. Gentili, "Bidirectional reflectance of oceanic waters: accounting for Raman emission and varying particle scattering phase function," *Appl. Opt.* **41**(30), 6289–6306 (2002).
46. C. M. Hu and K. J. Voss, "In situ measurements of Raman scattering in clear ocean water," *Appl. Opt.* **36**(27), 6962–6967 (1997).
47. J. W. Wei, Z. P. Lee, and S. L. Shang, "A system to measure the data quality of spectral remote sensing reflectance of aquatic environments," *J. Geophys. Res.: Oceans* **121**, 8189–8207 (2016).
48. K. E. Taylor, "Summarizing multiple aspects of model performance in a single diagram," *J. Geophys. Res.* **106**(D7), 7183–7192 (2001).
49. W. Zhou, J. F. Lin, and R. H. Ma, "Effects of forward models on the semi-analytical retrieval of inherent optical properties from remote sensing reflectance," *Appl. Opt.* **58**(13), 3509–3527 (2019).
50. Z. P. Lee, J. W. Wei, K. Voss, M. Lewis, A. Bricaud, and Y. Huot, "Hyperspectral absorption coefficient of 'pure' seawater in the range of 350–550 nm inverted from remote sensing reflectance," *Appl. Opt.* **54**(3), 546–558 (2015).
51. X. L. Yu, Z. P. Lee, J. W. Wei, and S. Shang, "Impacts of pure seawater absorption coefficient on remotely sensed inherent optical properties in oligotrophic waters," *Opt. Express* **27**(24), 34974–34984 (2019).
52. S. Betancur-Turizo, A. González-Silvera, E. Santamaría-del-Ángel, J. Tan, and R. Frouin, "Evaluation of Semi-Analytical Algorithms to Retrieve Particulate and Dissolved Absorption Coefficients in Gulf of California Optically Complex Waters," *Remote Sens.* **10**(9), 1443–1460 (2018).
53. A. Bricaud, H. Claustre, J. P. Ras, and K. Oubelkheir, "Natural variability of phytoplanktonic absorption in oceanic waters: Influence of the size structure of algal populations," *J. Geophys. Res.: Oceans* **109**(C11), C11010 (2004).
54. L. R. Favaretto, N. Rudorff, M. Kampel, R. Frouin, R. Röttgers, D. Doxaran, H. Murakami, and C. Dupouy, "Bio-Optical Characterization and Ocean Colour Inversion in the Eastern Lagoon of New Caledonia, South Tropical Pacific," *Remote Sens.* **10**(7), 1043–1073 (2018).

55. G. F. Wang, W. X. Cao, D. Z. Xu, S. Liu, and J. L. Zhang, "Variations in specific absorption coefficients of phytoplankton in northern South China Sea," *J. Trop. Oceanogr.* **24**, 1–10 (2005).
56. P. J. Werdell and S. W. Bailey, "An improved in-situ bio-optical data set for ocean color algorithm development and satellite data product validation," *Remote Sens. Environ.* **98**(1), 122–140 (2005).
57. M. Marrari, C. M. Hu, and K. Daly, "Validation of SeaWiFS chlorophyll a concentrations in the Southern Ocean: A revisit," *Remote Sens. Environ.* **105**(4), 367–375 (2006).
58. C. M. Hu, Z. P. Lee, and B. Franz, "Chlorophyll a algorithms for oligotrophic oceans: A novel approach based on three-band reflectance difference," *J. Geophys. Res.: Oceans* **117**, C1 (2012).
59. B. Kumari, "Comparison of high performance liquid chromatography and fluorometric ocean colour pigments," *J. Indian Soc. Remote Sens.* **33**(4), 541–546 (2005).
60. R. A. Reynolds, D. Stramski, and G. Neukermans, "Optical backscattering by particles in Arctic seawater and relationships to particle mass concentration, size distribution, and bulk composition," *Limnol. Oceanogr.* **61**(5), 1869–1890 (2016).
61. C. D. Mobley, *Light and Water: Radiative Transfer in Natural Waters*. (Academic Inc., 1994).